AGU PUBLICATIONS

JGR

Journal of Geophysical Research: Earth Surface

RESEARCH ARTICLE
10.1002/2015JF003511

Special Section:
Glacier Surging and Ice Streaming

Dynamics of surge-type glaciers in West Kunlun Shan, Northwestern Tibet

Takatoshi Yasuda[1] and Masato Furuya[1]

[1]Department of Earth and Planetary Sciences, Hokkaido University, Sapporo, Japan

Abstract Here we examine 31 glaciers in the West Kunlun Shan of the northwestern Tibetan Plateau and identify 9 as surge type. The method is based on satellite synthetic aperture radar and Landsat optical images, the former going back to 1992, the latter to 1972. To identify surge-type glaciers, we consider temporal changes in velocity, changes in glacier terminus position, propagation of a surge bulge, presence of looped and/or contoured medial moraines, and extensive crevassing. Other than the nine surge-type glaciers, we identify two that have likely surged, and six that may be surge type. But no glacier surges more than once during the observation period, meaning that the recurrence interval exceeds 42 years. In addition, we examine the evolution of the surface velocities at two surging glaciers with the unprecedented temporal resolution of down to 11 days over ~7 years. The results show clear seasonal modulations by as much as ~200% in early winter against those in early summer. This seasonal modulation in surface velocity suggests the presence of surface meltwater that reroutes through the englacial and subglacial drainage systems. Thus, our findings suggest that the hydrological processes originating in the surface meltwater play an important role in maintaining the yearlong active surging phase.

Key Points:
- Inventory and characteristics of surge-type glaciers in West Kunlun Shan
- Velocity changes of surging glaciers with unprecedented temporal resolution
- The winter speedup at the polythermal glacier surging

Supporting Information:
- Text S1 and Table S1

Correspondence to:
T. Yasuda,
hawkyear@frontier.hokudai.ac.jp

Citation:
Yasuda, T., and M. Furuya (2015), Dynamics of surge-type glaciers in West Kunlun Shan, Northwestern Tibet, *J. Geophys. Res. Earth Surf.*, *120*, doi:10.1002/2015JF003511.

Received 17 MAR 2015
Accepted 3 NOV 2015
Accepted article online 9 NOV 2015

1. Introduction

Due to the global warming trend since the twentieth century, meltwater from melting snow cover and glaciers is estimated to significantly contribute to the global sea level rise [*Meier et al.*, 2007; *Gardner et al.*, 2013]. In the high-mountain Asia (HMA) region, a mass loss of about 30 Gt/yr was estimated for the period between 2003 and 2009 [*Gardner et al.*, 2013]. However, the remoteness of the region has resulted in a paucity of ground-based glaciological observations, and the spatial and temporal coverage of satellite remote sensing has been sparse. Thus, details of the glacier changes in the HMA over the past several decades still contain large uncertainties [*Bolch et al.*, 2012; *Gardner et al.*, 2013].

Within the HMA lies the West Kunlun Shan (WKS), one of the highest-elevation areas on Earth (Figure 1). Due to its harsh environment, even fewer ground-based glaciological studies have been done here [*Zhang and Jiao*, 1987; *Zhang et al.*, 1989; *Thompson et al.*, 1995]. As such, satellite remote sensing techniques have been used to evaluate the temporal changes in WKS glaciers. For example, *Shangguan et al.* [2007] used Landsat images from 1970 to 2001 to find a slight reduction (0.4%) in the total glaciated area (2711.57 km^2). However, *Gardner et al.* [2013], using differences between ICESat/GLAS laser altimetry data and the digital elevation maps from Shuttle Radar Topography Mission, found a mass gain in WKS glaciers, with equivalent elevation changes of 0.17 ± 0.15 m/yr from 2003 to 2009. Less clear is the glacier dynamics in the WKS, but radar-image analyses have been used to identify surge-type glaciers there [*Yasuda and Furuya*, 2013].

Surge-type glaciers exhibit cyclic behavior, of period decades to centuries, between their quiescent and active phase [*Meier and Post*, 1969; *Raymond*, 1987; *Harrison and Post*, 2003]. In their active phase, when they accelerate to an amount at least 10 times that in their quiescent phase, they are considered to be surging. During a surge, a significant volume of the entire ice mass moves downstream, leading to dramatic changes in the surface height and sometimes terminus position, as well as forming newer crevasses and looped moraines. In the longer quiescent phase, a surge-type glacier flows slowly or becomes stagnant in the downstream area, leading to ice mass accumulation upstream. The imbalanced flow causes retreat and thinning in the lower part.

Glacier mass balance is usually estimated by assuming only nonsurge-type glaciers whose dynamics are altered only by long-term climate changes. Thus, the identification of surge-type glaciers in the WKS can

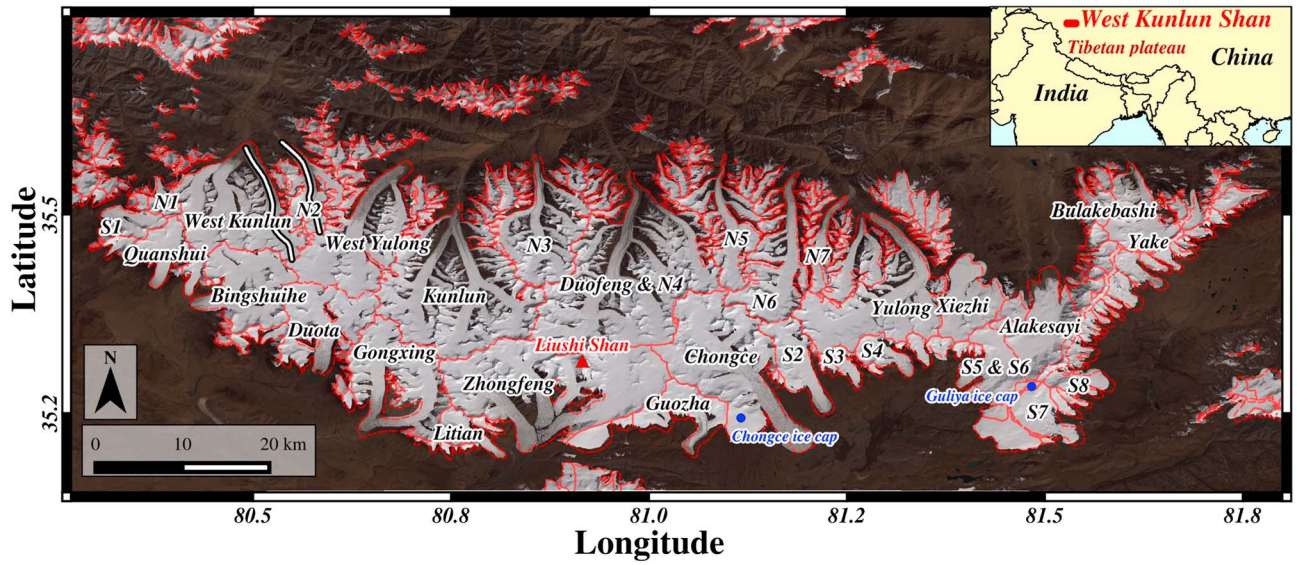

Figure 1. West Kunlun Shan on Landsat 8 true color image from 27 September 2013. Red dashed lines show glacier outlines from the Randolph glacier inventory version 4.0 [*Pfeffer et al.*, 2014]. Glacier names are from National Snow and Ice Data Center world glacier inventory [*Ma et al.*, 1989; *Zheng et al.*, 1989]. Those glaciers with N or S indicate unnamed glaciers in the northern and southern slope, respectively. The white lines at the West Kunlun and the N2 glaciers denote profile lines used for Figures 5 and 6.

alter our interpretation of mass balance studies in the region [*Yde and Paasche*, 2010]. For instance, a significant increase of ablation at nonsurge-type glaciers would suggest overall recession of the frontal positions. However, such an increase at surge-type glaciers reflects only a snapshot of the normal surge cycle.

Two types of surge can occur, Alaskan type and Svalbard type. Alaskan-type surges abruptly initiate in winter and terminate in summer with a short active phase (1–3 years) [*Kamb et al.*, 1985; *Kamb*, 1987; *Harrison and Post*, 2003; *Lingle and Fatland*, 2003; *Eisen et al.*, 2005; *Burgess et al.*, 2012]. On the other hand, Svalbard-type surges gradually initiate and terminate in any season with a longer active phase (>3 years) [*Fowler et al.*, 2001; *Murray et al.*, 2003; *Quincey et al.*, 2011; *Sund et al.*, 2014]. Their maximum flow velocities and recurrence intervals also differ, with the Svalbard-type surge having much lower maximum flow velocity but longer recurrence interval (several decades or more). These different behaviors indicate different physical mechanisms, specifically, hydrological regulation for the Alaskan type and thermal regulation for the Svalbard type. However, we use here the terms "Alaskan type" and "Svalbard type" solely to distinguish the different styles of surging, not the underlying mechanism. In the WKS, the results here suggest a hydrological mechanism, and yet the long duration and recurrence interval are that of the Svalbard type.

Previous work in the WKS has identified four surge-type glaciers [*Yasuda and Furuya*, 2013]. But that study covered only a short time period, covering changes in the flow speed from 2003 to 2011. To further extend the analysis period back into the 1990s, we add here ERS-1 and ERS-2 satellite data, and to extend from 2012, we add TerraSAR-X data. We also use Landsat optical images since 1972 to examine any features that could be associated with surges such as changes in glacier terminus position, surface crevassing, and folded moraines. Finally, to the coverage, we add here a new glacier, bringing the total number to 31 examined glaciers.

The first objective of this study is thus to identify the distribution and characteristics of surge-type glaciers in the WKS, with the aim to help improve present and future mass balance studies.

The second objective is to examine the evolution of surface velocity at surging glaciers in the WKS with temporal resolution as fine as 11 days, with the aim to better understand the generation mechanisms of surging at polythermal glaciers.

2. Study Area

Most WKS peak elevations exceed 6500 m above sea level (asl), the highest peak being Luishi Shan at 7167 m (Figure 1). The region has 278 glaciers, with a total area of 2711.57 km^2 in 1970 [*Shangguan et al.*, 2007]. The debris-covered area is less than 3% [*Scherler et al.*, 2011]. *Zheng et al.* [1989] indicated the presence of the

Table 1. Satellite SAR Sensors and Basic Properties

Satellite/Sensor	ERS1-2/AMI	ENVISAT/ASAR	ALOS/PALSAR	TerraSAR-X
Authorities	ESA	ESA	JAXA	DLR
Band (wavelength)	C (5.66 cm)	C (5.62 cm)	L (23.61 cm)	X (3.01 cm)
Data coverage	1992 and 1996	2003–2007	2007–2011	2012–2014
Mode	Image/tandem	Image	FBS/FBD[b]	Stripmap
Spatial resolution[a](m)	7.9 × 3.9	7.8 × 4.05	4.68 / 9.36 × 3.14	0.9 × 2.05
Revisit period	35/1 days	35 days	46 days	11 days
Parameters for offset tracking				
Window size pixels[a]	128 × 256	35 × 70	60 × 90	256 × 256
Step pixels[a]	16 × 20	7 × 14	12 × 18	50 × 25
SNR threshold	>2.0	>3.0	>3.0	>2.0
Estimated uncertainties				
Mean (m/yr)	40.6 / 1.2×10^4	44.1	30.2	41.7
Median (m/yr)	36.4 / 1.3×10^4	41.1	26.4	42.4
Standard deviation (m/yr)	23.5 / 0.5×10^4	23.7	19.1	23.9

[a]Range times azimuth.
[b]Fine Beam Single polarization and Fine Beam Dual polarization.

subglacial debris layer with a ~30 m thickness near the Guliya ice cap (Figure 1). Along the main ridge, the WKS is divided into south and north slopes. On the southern slope, the elevation gradually lowers toward the plateau surface, and no glaciers develop below 5200 m [*Zhang and Jiao*, 1987]. In contrast, the northern slope has relatively long, steep glaciers that flow into steep-walled valleys, and some glaciers develop below 5000 m [*Zhang et al.*, 1989]. Of all glaciers in the HMA, those in the WKS have the most continental climate, as the region is the coldest and driest around the Tibetan plateau. Here the annual average precipitation and temperature near the equilibrium line altitude (5930 m) is about 300 mm and −13.9°C, respectively [*Zhang et al.*, 1989]. Accumulation and ablation mostly occur in the summer season from May to August [*Zhang et al.*, 1989; *Maussion et al.*, 2014], influenced partly by the East Asian monsoon after the westerly jet shift to the north in April. Although the latitudes and altitudes are similar to those in the Karakoram to the west, the glaciers in the WKS generally have a smaller elevation range, and thus are not as steep as those in the Karakoram. A further difference with the Karakoram is in the accumulation season. In western Karakoram regions, winter accumulation dominates [*Maussion et al.*, 2014], whereas in the central Karakoram, accumulation occurs almost equally in summer and winter [*Hewitt*, 2013].

3. Data

3.1. Satellite Synthetic Aperture Radar Images

We processed the satellite synthetic aperture radar (SAR) data sets to derive glacier velocity maps and their temporal changes. Different analysis periods relied on different SAR data sets. We list the characteristics of these SAR sensors in Table 1. (See supporting information Table S1 for details of the SAR data sets.) For data from 1992 and 1996, we used data from ERS-1 and ERS-2, operated by the European Space Agency (ESA). They carried the Active Microwave Instrument (AMI) operating in C band (5.66 cm wavelength), which observed a given region every 35 days. In addition, ESA ran a ERS-1/2 tandem mode with only 1 day temporal separation. We used the tandem data in 1996 to detect an extremely rapid flow during the active surging phase at the Chongce glacier. For 2007 to 2012, we used the Phased Array-type L band (23.6 cm wavelength) Synthetic Aperture Radar (PALSAR) on board the Advanced Land Observation Satellite (ALOS), which was operated by the Japan Aerospace Exploration Agency (JAXA). For data from 2012, we used the TerraSAR-X (TSX) stripmap mode data, which used X band microwave (3.01 cm wavelength). The TSX was operated by Deutsches Zentrum für Luft- und Raumfahrt (DLR). The revisit period of the TSX is nominally every 11 days. However, some sensors were operated at the study area with a longer-than-nominal revisit period.

3.2. Landsat Images

Landsat (LSAT) satellite images from NASA go back to 1972. Thus, we use them to extend our analysis period and to detect surface features that were indicative of surge-type glaciers. From 1972 to 1983, the multispectral

scanner on LSAT1, LSAT2, and LSAT3, produced data in four spectral bands ranging from visible green to near infrared, with a ground resolution of 80 m. From 1982 to 2013, the thematic mapper (TM) on LSAT4 and LSAT5 produced data in six bands ranging from visible blue to IR, all with an improved spatial resolution of 30 m, and also one thermal band with a resolution of 120 m. From 1999, the enhanced thematic mapper plus on LSAT7 produced data in six bands similar to the TM sensor, and also had thermal band, with the higher resolution of 60 m. LSAT7 also had an additional panchromatic band with 15 m resolution. But failure of the scan line corrector in May 2003 caused a loss of all subsequent data. From 2013, the operational land imager (OLI) on LSAT8 produced data in nine bands plus two bands in the thermal infrared sensor (TIRS). The OLI resolution ranges from 15 m of panchromatic to 30 m, whereas TIRS has 100 m resolution.

4. Methods

4.1. Measurement of Glacier Surface Velocity

We used the Gamma [*Wegmüller and Werner*, 1997] software package to process the SAR data sets. The shortest temporal pair was chosen to avoid the temporal decorrelation that can arise from fast flow or melting of the ice surface. In preprocessing, the pair was coregistrated based on each orbit data. Over rugged terrain, the separation between satellite orbital paths can lead to an artificial offset [*Michel et al.*, 1999; *Kobayashi et al.*, 2009]. To reduce this artifact, we applied an elevation-dependent correction with the SRTM4 DEM (Shuttle Radar Topography Mission digital elevation model; http://srtm.csi.cgiar.org) [*Jarvis et al.*, 2008]. To detect glacier flow, we used the offset tracking method [*Strozzi et al.*, 2002; *Luckman et al.*, 2007; *Yasuda and Furuya*, 2013]. The algorithm is based on maximizing the cross correlation between the master and slave images at the local pixel windows, so that we can derive the local image offsets as well as the signal-to-noise ratio (SNR). The lower the SNR, the lower the coherence between the two images, and the derived offsets are less reliable. When the SNR went below an assigned threshold, we discarded them as missing data. See Table 1 for the specific parameters.

Depending on the spatial resolution of each satellite, we chose the range and azimuth steps to obtain a final pixel size of ~50 m × 50 m. The tracking window size was 5 times that of the steps, except for TSX data. (TSX data has 256 × 256 pixels to catch the faster movement of surging glaciers.) The offsets were geocoded onto UTM coordinates with ~50 m × 50 m ground resolution and normalized to meters per year. We manually removed the unreliable offsets based on their magnitude. This removal used a glacier-area mask based on a semiautomatic algorithm with LSAT8 imagery [*Hendriks and Helsinki*, 2007].

To estimate velocity errors, we measured the offsets on stable ground (off glacier) [*Pritchard*, 2005; *Abe and Furuya*, 2015] and assumed a linear temporal velocity change. The resulting errors in the velocity were 20–40 m/yr (Table 1) with the exception of tandem pairs; this is due to our assumption of a linear velocity change over the 1 day interval.

4.2. Measurement of Changes in Terminus Position

To quantify the changes in glacier terminus positions, we used a box measurement method described in *Moon and Joughin* [2008]. Then following the approach by *McNabb and Hock* [2014], we manually digitized terminus outlines using false-color images from the bands in LSAT1 to LSAT8 as well as SAR intensity images. From these outlines, we used QGIS software (http://www.qgis.org) to manually delineate a centerline and terminus outline for each of the 31 major glaciers and 2 separate branches in the WKS.

4.3. Identification of Surge-Type Glaciers

To help distinguish the surge-type glaciers, we classified each glacier as one of the following four types [after *Copland et al.*, 2003]: (1) Confirmed: active surge phase observed, and many distinct surged features; (2) likely surged: active phase not observed, but distinct surged features with looped and contoured medial moraines; (3) possibly surged: active phase not observed, but distinct surged features without the medial moraines; and (4) Nonsurge: no surged features present.

"Confirmed," or type 1, cases can be most easily identified from direct evidence during the active phase, for example, observation of significant temporal changes in the flow speed, propagation of the surge bulge, and rapid advance with heavy crevassing [*Clarke et al.*, 1986; *Copland et al.*, 2003; *Dowdeswell et al.*, 2007]. The flow-velocity data to identify the active surges in the WKS are based on those in *Yasuda and Furuya* [2013].

A surge-type glacier in its quiescent phase needs careful inspection because surged features can appear on nonsurge-type glaciers. We thus used multiple criteria to distinguish surge-type from nonsurge-type glaciers

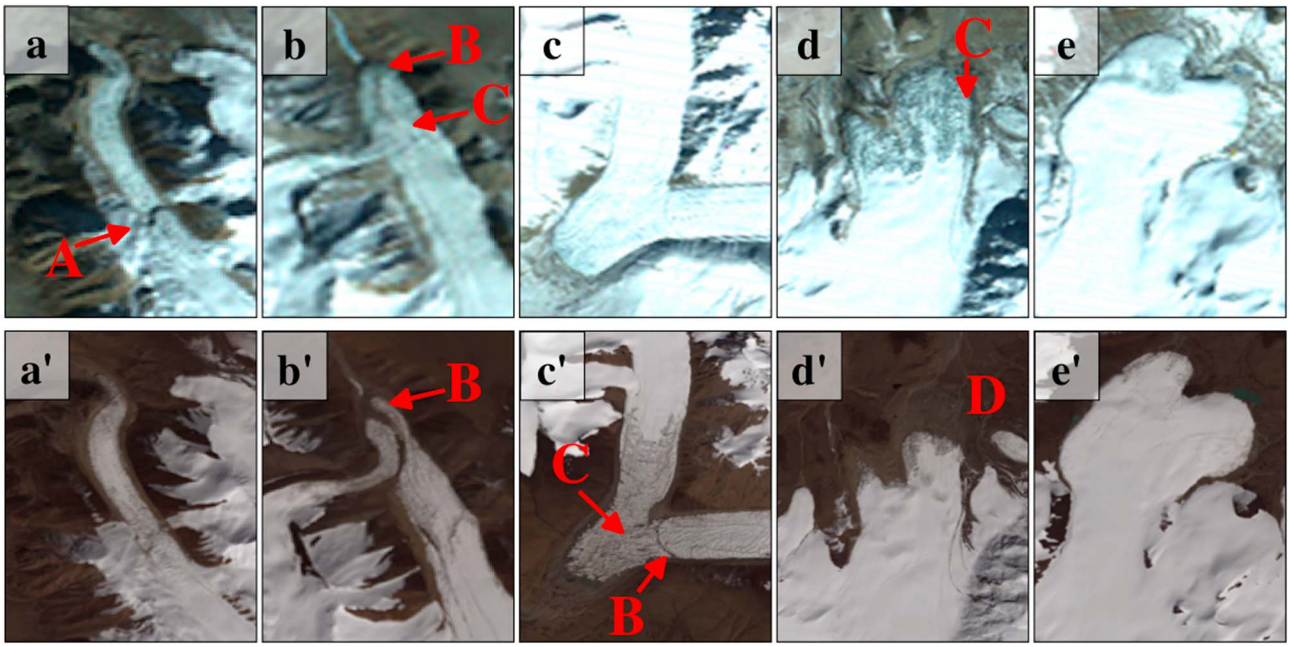

Figure 2. Examples of surge features on the glacier surface. The glacier sources and their types are (a) Bulakebashi (confirmed), (b) Yake (likely), (c) Gongxing (likely), (d) Alakesayi (possibly), and (e) Xiezhi (nonsurge). The Landsat images are from 1972 (Figures 2a–2e) and in (a'–e') 2013. Surge features: a surge bulge (A), moraines (B), crevassed surface (C), and rapid retreat in the terminus (D).

[*Copland et al.*, 2003; *Grant et al.*, 2009]. See Figure 2 for examples of such surged features. For the "likely surged," or type 2, cases, we looked for looped and contoured medial moraines. Such moraines reliably indicate past surging events [*Meier and Post*, 1969]. However, on the almost debris-free glaciers in the WKS [*Scherler et al.*, 2011], such moraines are not always clearly preserved. For the "possibly surged," or type 3, case, we looked for two features that can form during the rapid terminus retreat. This retreat commonly leaves (1) stagnant ice in the lower part and (2) a heavily crevassed surface [*Meier and Post*, 1969; *Copland et al.*, 2003; *Burgess et al.*, 2013].

5. Results

5.1. Categorization of the Glaciers in the WKS

Among the examined 31 glaciers in the WKS from 1972 to 2014, we find 9 glaciers to have surged (type 1), 2 to have likely surged (type 2), and 6 to have possibly surged (type 3). The remaining 14 we classify as nonsurge type (type 4). See Figure 3 for their locations. For the surge-type glaciers, the figure also shows when the surging occurred. The criteria that determine the surge-type and likely surged glaciers appear in Table 2.

Of the nine surge-type glaciers, four glaciers exhibit advancing signals during 1972–1992, whereas the other five increase their flow speed during 1992–2014 (Figure 3 and Table 2). The two glaciers that likely surged show neither velocity changes nor terminus changes but exhibit surged features with the looped and contoured medial moraines (Figures 2b and 2c). The six glaciers that possibly surged show significant changes in their terminus positions (Figure 4b). For instance, at the Alakesayi glacier, the heavily crevassed area indicates a rapid retreat (Figure 2d). The other 14 glaciers show no features associated with surging, and their terminus positions are almost stationary over time (Figure 4c).

To further investigate the differences in the glacier attributes between surge-type and nonsurge-type glaciers [*Clarke*, 1991; *Jiskoot et al.*, 1998; *Grant et al.*, 2009], we average data of Randolph Glacier Inventory version 4.0 (RGI4.0) by *Pfeffer et al.* [2014] to compare the geometric qualities of the four categories. Moreover, because the mountain shape significantly differs between both slopes [*Zhang and Jiao*, 1987; *Zhang et al.*, 1989], we also separate each category by northern and southern slope.

As shown in Table 3, surge-type glaciers occur on both northern and southern slopes but tend to have larger areas and longer lengths. In particular, areas of surge type exceed nonsurge types 137.3 ± 93.3 km^2 to 34.7 ± 23.5 km^2, whereas lengths of surge type exceed nonsurge types 20.6 ± 6.4 km to 10.6 ± 3.8 km.

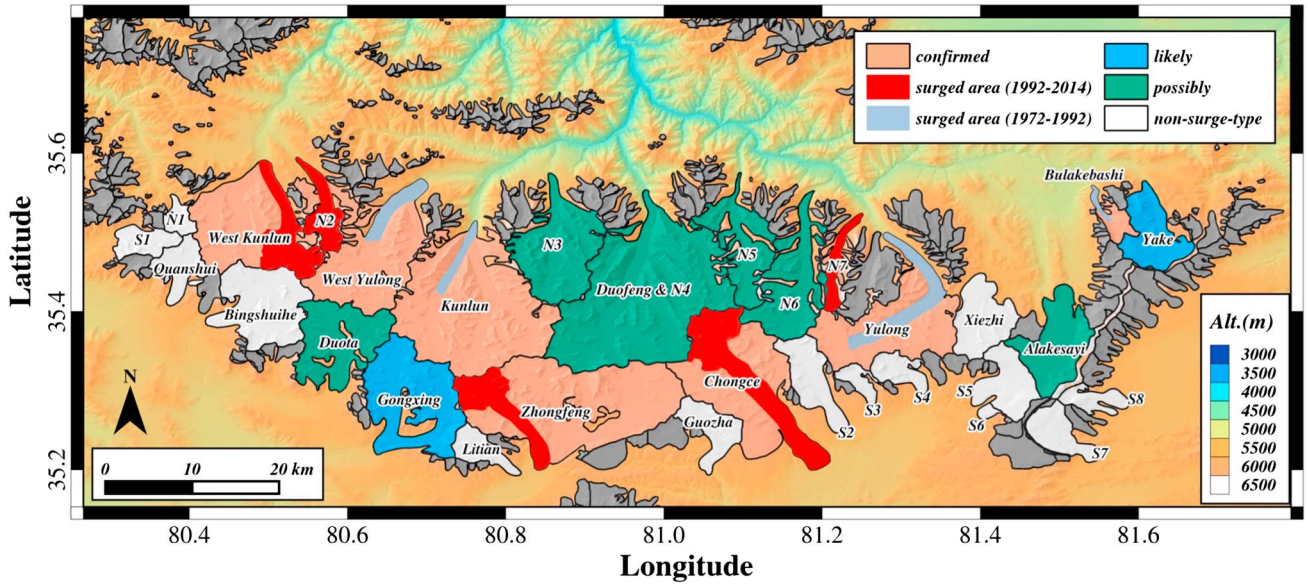

Figure 3. Distribution of surge-type glaciers and nonsurge-type glaciers. Glacier outlines are here based on RGI v4.0. Each category is filled with colors indicated in the top right legend. Surging areas are distinguished with different colors for before versus after 1992. Gray shaded glaciers were not examined in this study.

5.2. Temporal Changes in Glacier Terminus Position

Consider the spatial and temporal changes in the glacier terminus positions. The amount of retreat and advance associated with the surge cycle ranges between −2.5 km and +2.0 km (Figure 4a). In contrast, at nonsurge-type glaciers, the terminus positions remain stationary to the measurement error of less than ±100 m (Figure 4c). However, no surge-type glacier repeats its active phase during 1972–2014, which indicates a recurrence interval in the WKS of longer than 42 years. Although seven glaciers advance during the analysis period, the availability of satellite images allows us to examine here the details in only four cases after 2000 (Figure 4a).

The Zhongfeng glacier on the southern slope rapidly advanced by up to 2.5 km between July 2003 and March 2005. Its rate increased to ~6.3 km/yr during July–November 2003 and then decreased to ~0.5 km/yr from November 2003 to March 2005 and then terminated. The other three advancing glaciers, all on the northern slope (Figure 3), have advanced more slowly than that of Zhongfeng but were still advancing in 2014.

Table 2. The List of Confirmed Surging and Likely Surged With Detected Surge Features[a]

Glacier Name	Type	RGIID	Surge date	Flow Speed (>200 m/yr)	Surge Bulge	Advancing	Crevassing	Moraines	Stagnant Ice	Crevassed Ice	Retreating (>500 m)
				Northern Slope							
West Kunlun	1	RGI30-13.38232	~2000–2014 (ongoing)	x		x	x	x		x	x
N2	1	RGI30-13.38152	~2000–2014 (ongoing)	x		x	x			x	x
West Yulong	1	RGI30-13.38255	<1972			x	x		x	x	x
Kunlun	1	RGI30-13.38303	early 1970s			x	x	x	x	x	x
N7	1	RGI30-13.38175	2000–2013 (on going)	x		x	x				x
Yulong	1	RGI30-13.38245	between 1977 and 1989			x	x		x	x	x
Bulakebashi	1	RGI30-13.38211	~1977–2000		x	x	x		x	x	
Yake	2	RGI30-13.38111						x		x	
				Southern Slope							
Gongxing	2	RGI30-13.38266						x	x	x	x
Zhongfeng	1	RGI30-13.38172	~2000–2007	x		x	x	x	x	x	x
Chongce	1	RGI30-13.38216	1990s	x		x	x		x	x	x

[a]RGIID: glacier ID from Randolph Glacier Inventory.

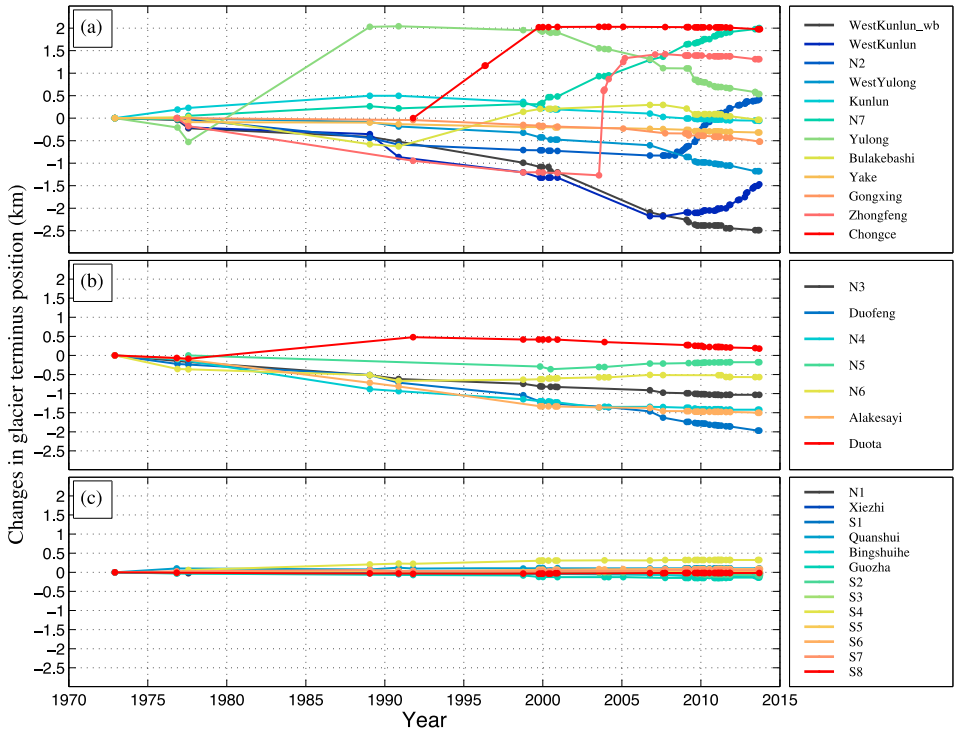

Figure 4. Temporal changes in glacier terminus positions from 1972 to 2014. (a) Confirmed and likely surged, (b) possibly surged, and (c) nonsurge type.

The slowest advance occurs with N7, a glacier whose terminus has been moving forward since 2000 at a rate of ~126 m/yr. The duration of advance at the N7 glacier is the longest. Since 1998, its terminus has been advancing, together with crevassing, in a northeastern direction but from 2003 turned north along a valley wall. Because of the narrower width, however, the detailed evolution of the surface features is uncertain.

The West Kunlun glacier has three branches whose front positions gradually retreated from 1972, with the eastern branch separating from the others in 2006. At the eastern branch, its terminus has been moving forward since November 2009. At the N2 glacier, its terminus has been moving forward since May 2008. The West Kunlun glacier and the N2 glacier changed their rates of advance. At the N2 glacier, for example, its terminus

Table 3. Averaged Geometric Data From RGI4.0 for the Categorized Glaciers in Figure 3[a]

		Count	Area (km^2)	Length (km)	Slope (deg)	zmin (m)	zmax (m)	zmed (m)
	N	7	112.2	19.1	11.8	5153.6	6591.1	6093.6
Confirmed	S	2	225.2	26.0	9.8	5326.0	6973.5	6131.0
	total	9	137.3 ± 93.3	20.6 ± 6.4	11.4 ± 2.5	5191.9 ± 119.5	6676.1 ± 208.4	6101.9 ± 89.4
	N	1	56.7	14.9	11.7	5251.0	6563.0	6099.0
Likely	S	1	127.7	20.4	11.5	5330.0	6654.0	6078.0
	total	2	92.2 ± 50.2	17.6 ± 3.9	11.6 ± 0.1	5290.5 ± 55.9	6608.5 ± 64.3	6088.5 ± 12.1
	N	5	131.1	23.0	13.8	4937.0	6745.8	6104.2
Possibly	S	1	92.3	15.4	9.7	5434.0	6392.0	6047.0
	total	6	124.6 ± 92.4	21.7 ± 5.7	13.1 ± 3.1	5019.8 ± 312.2	6686.8 ± 165.7	6094.7 ± 104.6
	N	2	35.8	9.6	10.7	5449.0	6347.0	5917.5
Nonsurge	S	12	34.5	10.8	10.3	5459.8	6492.1	5991.0
	total	14	34.7 ± 23.5	10.6 ± 3.8	10.4 ± 2.5	5458.2 ± 61.7	6471.4 ± 167.3	5980.5 ± 96.6

[a]"N" or "S" means that glaciers on the northern/southern slope.

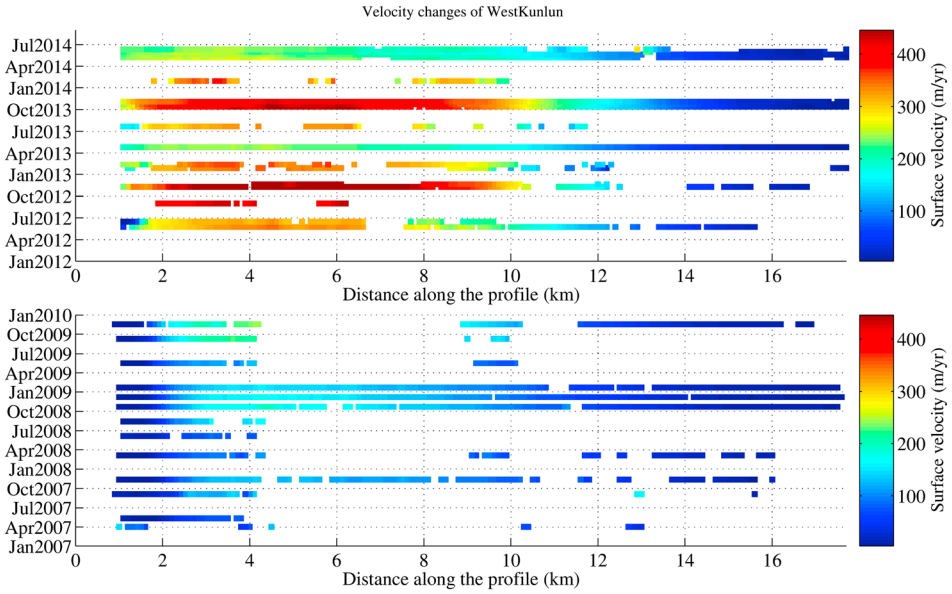

Figure 5. Spatial-temporal changes of the surface velocities at the West Kunlun glacier. The profile-line location is marked in Figure 1. The left edge is near the terminus, the right upstream. The glacier's total length is 16.5 km.

advanced at a rate of ~227 m/yr during May 2008 to August 2009, accelerating to ~460 m/yr during August 2009 to November 2010 and then slowing down to ~130 m/yr from November 2010.

Consider the possibly surged (type 3) glaciers. These show variations in their terminus positions ranging between −2.0 and +0.5 km (Figure 4b). For example, the N3 glacier gradually retreated by 1.0 km during 1972–2013. The Duofeng and N4 glaciers merged in the 1970s, probably due to past surging at the N4, but their termini rapidly shrunk and separated. Then their termini positions retreated, the Duofeng by 2 km and N4 by 1.3 km. The N5, the N6, and the Alakesayi glaciers also gradually retreated from the 1970s, but their terminus positions were nearly stationary until about 2000 when they may slightly advance. The Duota glacier advanced slightly by 1992, but then retreated by 2013, probably due to an interaction with its proglacial lake.

The terminus positions of nonsurge-type glaciers are stationary during our observation period (Figure 4c). Except for the S4 glacier, whose terminus gradually advances 300 m by 2000, other termini remain stationary within ±100 m.

5.3. Winter Speedup of the Surging Glaciers

The active phase of the two surging glaciers show velocities that are faster in winter than those in summer. Figures 5 and 6 show the spatial-temporal changes in the longitudinal velocity profile at the West Kunlun glacier and the N2 glacier, respectively. Because of the limited temporal resolution, the exact dates their active surging phase began are unknown, but both glaciers were in their quiescent phase before 2000 when the terminus positions had been receding (Figure 4a). As both glaciers were still in the active phase by 2014, their active phase lasts longer than 5 years. In both cases, the peak velocity occurs near the lowermost part of the glaciers. Although these findings were consistent with those reported at the Karakoram glacier surge [*Quincey et al.*, 2011], the finer temporal resolution images clearly demonstrate the seasonal modulation of the flow velocities. For subpolar/polythermal surging glaciers, such seasonal modulation had not been previously reported.

At the West Kunlun glacier in Figure 5, the peak velocity is about 130 m/yr in 2007–2008, but increases year by year up to 170 m/yr in 2008–2009, 200 m/yr in 2009–2010, 450 m/yr in 2012–2013, and 500 m/yr in 2013–2014. All these peak velocities occur from the late fall to winter season. Meanwhile, the velocities in April to June appear slower than those in late fall to winter. For example, the summer velocities at the 2 km point in 2008, 2012, and 2013 are ~100 m/yr, ~300 m/yr, and ~250 m/yr. This shows a nearly 200% seasonal change in the velocity amplitude.

Similarly, for the N2 glacier, the summer season of 2013 shows a clear slowdown in Figure 6, with a ~200% velocity increase in winter. But we cannot recognize an interannual velocity increase at the N2 glacier.

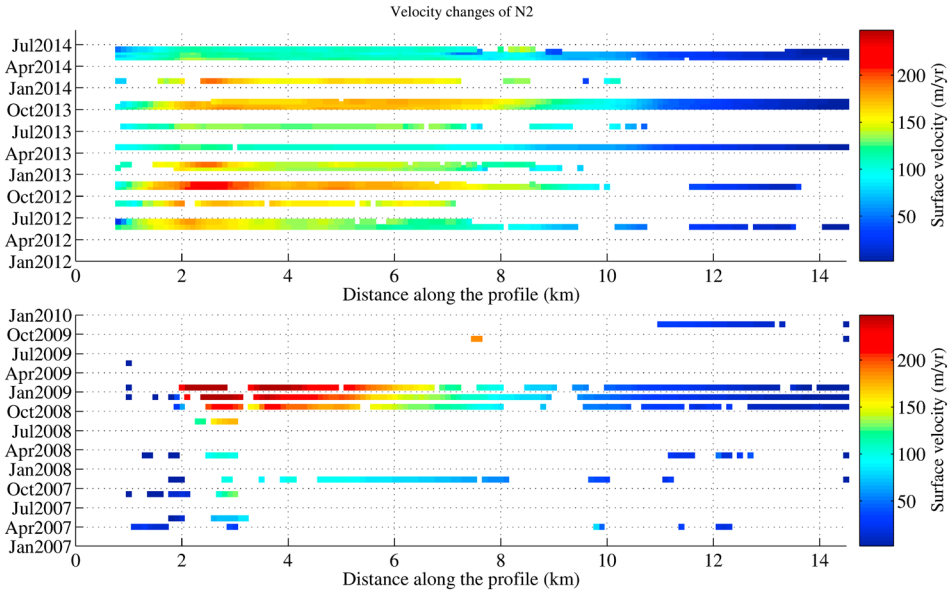

Figure 6. Same as Figure 5 except for the N2 Glacier. The glacier's total length is 13.7 km.

6. Discussions

6.1. Implication for Previous Studies on Mass Balance

Most previous studies estimated glacier mass balance in the WKS via changes in glacier area, length, or ice thickness without considering the presence of surge-type glaciers. The reported reduction (0.4%) of the glacier area by *Shangguan et al.* [2007] may be reconciled by the movements of the terminus at the surge-type glaciers.

While the ICESat altimeter data indicated that the glaciers had been thickening during 2003–2009 [*Gardner et al.*, 2013], the glacier surges caused significant surface lowering in the accumulation area [*Neckel et al.*, 2014]. Our results indicate that the ICESat footprints cover five quiescent surge-type glaciers, and that two surge events, especially the surging at the Zhongfeng glacier, cause the heterogeneous elevation changes. In view of the widely distributed surge-type glaciers, the limited ICESat tracks are not good enough to reliably examine the effect of climate changes upon the regional mass balance in the WKS. Such an examination requires more complete spatial coverages in the glacier elevation change data [e.g., *Gardelle et al.*, 2013].

6.2. Characteristics of the Surge-Type Glaciers

The surge-type glaciers in the WKS tend to have larger areas and longer lengths than nonsurge-type glaciers (Table 3), which is largely consistent with previous studies [e.g., *Clarke et al.*, 1986; *Clarke*, 1991; *Jiskoot et al.*, 1998; *Grant et al.*, 2009]. The nonsurge-type glaciers generally have smaller areas and shorter lengths, and are located mainly on the southern slope, and thus generally have higher terminus elevations than those at the northern slope. Even if the numerous unexamined smaller, shorter glaciers in Figure 1 were all surge type, they would add little to the total area of surge-type glaciers because they occupy less than 10% of the total WKS area. Thus, the total area of surge-type glaciers in the WKS comes mainly from the larger, longer glaciers. Differences in topography may affect glacier-termini positions between the northern and the southern slopes. On the northern slope, relatively long, steep glaciers can flow into deep incised valleys below 5000 m asl [*Zhang et al.*, 1989]. On this slope, the marked retreats of the terminus would represent the rapid depletion of the advanced terminus by the past surge due to the increase in ablation. The past surging and subsequent retreat at the Yulong glacier might support the inference. In contrast, on the southern slope, there are no deeply incised valleys and the elevation gradually decreases to a relatively flat plateau. Here Piedmont glaciers dominate, with none developed below 5200 m asl [*Zhang et al.*, 1989]. As such, although we could discern the retreat of the frontal position at the Zhongfeng glacier prior to its surging (Figure 4a), the ablation on the southern slope could be smaller, and the retreat rate slower, than that on the northern slope, and the remnant ice due to past surge might exist until next surge.

The gradual development of ice speed, as well as the durations of the active and quiescent phases, here is similar to those in Svalbard [*Murray et al.*, 2003] and the Karakoram [*Quincey et al.*, 2011; *Hewitt*, 2013] but differ from those of the Alaskan-type surge [*Kamb et al.*, 1985]. In addition, the peak velocities in the WKS (0.2–1 km/yr) [*Yasuda and Furuya*, 2013] are much smaller than that at the Variegated glacier in Alaska (~23.7 km/yr) [*Kamb et al.*, 1985] and at the Sortebræin East Greenland (~8.8 km/yr) [*Pritchard*, 2005], but they are consistent with those measured at Monocobreen in Svalbard (~1.8 km/yr) [*Murray et al.*, 2003] and at the Khurdopin glacier in the Karakoram (~1 km/yr) [*Quincey et al.*, 2011].

We argue below, however, that glacier surging at the N2 and the West Kunlun glaciers could be influenced by the input of surface meltwater and subsequent evolution of the drainage system inside and below the ice body, a mechanism similar to that of surge-type glaciers in Alaska [*Kamb et al.*, 1985].

6.3. Implications for the Surge Mechanisms at Polythermal Glaciers

Till deformation has been suggested as an important process for surge generation [e.g., *Murray et al.*, 2000; *Truffer et al.*, 2000]. For instance, the findings of *Truffer et al.* [2000] suggest large-scale mobilization of subglacial sediment during the active surging at Black Rapid Glacier in Alaska. However, according to the Coulomb-plastic rheology for till deformation [e.g., *Clarke*, 2005], a high basal water pressure is necessary for substantial till deformation. Therefore, regardless of the presence of a till layer beneath some glaciers in the WKS [*Zheng et al.*, 1989], the surge generation mechanism should include a process that can supply a high basal water pressure.

In terms of the generation processes of high-pressure basal water, the mechanisms of hydrological regulation and the thermal regulation are entirely different. In the hydrological regulation mechanism, which is based mainly on Alaskan-type surges [*Kamb et al.*, 1985; *Kamb*, 1987; *Harrison and Post*, 2003; *Lingle and Fatland*, 2003; *Eisen et al.*, 2005; *Burgess et al.*, 2012], the basal water originates in surface meltwater as evidenced by the seasonal evolution. But in the thermal regulation mechanism, which is based on the observations of surges at polythermal glaciers in Svalbard [*Fowler et al.*, 2001; *Murray et al.*, 2000, 2003], the basal water comes entirely from the bottom of the ice. This source of melt is thought to be supplied by pressure melting of the overburden ice as the accumulation zone receives more ice over time. Upon the initiation of basal slip, frictional heating due to the ice motion is thought to generate additional meltwater. Although recent studies indicate the presence of both Alaskan-type and Svalbard-type surges in the same geographical locations, such as in East Greenland [*Jiskoot et al.*, 2001; *Pritchard*, 2005; *Jiskoot and Juhlin*, 2009], the indications are based on the differences in the durations of active and quiescent phases, the peak velocities, and the presence or absence of discharge events.

In the WKS, the observed summer slowdown and winter speedup during the active surging phase are significant in terms of the surge mechanisms at polythermal glaciers, because they are reminiscent of the Alaskan type rather than the Svalbard type. While the temporal durations of the entire active phase are certainly longer than those in Alaska, the presence of the seasonal modulation in the surface velocities demonstrates the effect of surface meltwater and suggests its rerouting through englacial and subglacial drainage system. The finding suggests a reconsideration of the origin of basal water in polythermal surge-type glaciers.

Surface velocity observations at other glaciers in the WKS indicate a variety of seasonal changes [*Yasuda and Furuya*, 2013]. The Duofeng glacier, 40 km east of the surging West Kunlun and N2 glaciers (Figure 1), also shows the well-known summer speedup and winter slowdown signals [*Yasuda and Furuya*, 2013], which may be understood using the standard summer speedup theory [*Schoof*, 2010; *Bartholomaus et al.*, 2011; *Werder et al.*, 2013]. On the other hand, at stagnant glaciers such as the Chongce glacier, there are few seasonal changes at the downstream near the terminus, which probably indicates either that the downstream is not thick enough to flow or is entirely frozen to the bed. As it is unlikely that surface meltwater production is spatially heterogeneous over the studied area, the diverse seasonal velocity evolution pattern suggests that the meltwater rerouting and discharge processes would differ by glacier and temporally evolve over time.

Concerning this meltwater rerouting, we consider the following processes. At the onset of the active surging phase, we assume that a linked-cavity drainage system has formed at the glacier bed [*Kamb*, 1987]. Porous deformable sediments [e.g., *Fowler et al.*, 2001] may also be present, supplying an inefficient drainage system. Moreover, their subsequent deformation and dilation would have the same mechanical impact on the basal water pressure as the linked-cavity system, increasing water storage [*Fowler et al.*, 2001]. Once the surge initiates, the cavity size on the leeward side of the bumpy bed should increase, generating more and more

interconnected cavities [*Iken and Truffer*, 1997] that might allow more water to be stored. Moreover, new crevasses form, which could deliver surface meltwater to the bed in summer. Despite the increase of meltwater influx, the increased cavity volume, as well as the crevasses, could store the water, leading to a decrease in water pressure and slower surface velocity in spring and summer.

Although this mechanism may seem contrary to the well-known spring-summer speedup mechanism [*Schoof*, 2010; *Bartholomaus et al.*, 2011; *Werder et al.*, 2013], consider that basal water pressure is not only proportional to the total englacial water volume but also has been argued to be inversely proportional to the macroscopic porosity [*Bartholomaus et al.*, 2011; *Bueler*, 2014]. Also, it is likely that the meltwater influx itself would be smaller than that at temperate glaciers, which could prevent channels from being developed. Because the tunnel-like channels might be absent, or only weakly developed, during the surge at the bed, the summer meltwater might not drain efficiently as in the usual summer speedup [*Schoof*, 2010; *Bartholomaus et al.*, 2011; *Werder et al.*, 2013]. As a result, a portion of the meltwater would remain until late fall to winter. During the absence of surface meltwater input, creep closure at both the bed and the crevasses could reduce the total volume of interconnected cavities and englacial water, increasing both the water pressure and overlying ice speed. Namely, the higher basal water pressure in winter would not arise from an increase of water input from the surface, but rather through a reduction of macroscopic porosity in the ice.

The WKS surge flow speeds are much slower than that observed at the Variegated glacier surge, which could be due to the smaller englacial and subglacial water volume inherent to the colder and drier climate. Hence, as long as the accumulation area has enough ice mass, the seasonal cycle during the surge may repeat, which could explain the longer duration of the active phase.

Abe and Furuya [2015] recently identified winter speedup signals at the quiescent polythermal surge-type glaciers in the Yukon, and, following a proposal of *Lingle and Fatland* [2003], suggested the importance of englacial storage for the speedup. For this storage, *Abe and Furuya* [2015] suggested basal crevasses [*Harper et al.*, 2010]; however, firn aquifers like those at temperate glaciers [*Fountain and Walder*, 1998] and ice sheets [*Forster et al.*, 2014] may also be a form of englacial storage at polythermal glaciers. But in contrast to the present findings, *Abe and Furuya* [2015] observed both the well-known summer speedup in the downstream and the winter speedup in the upstream. The absence of summer speedup signals in Figures 5 and 6 suggests that the standard summer speedup mechanisms do not apply to the surging glaciers in the WKS. The lack of a summer speedup supports the absence of channel-like drainage systems, but it could also be partly due to the insufficient meltwater influx. However, in winter, the speedup occurs over broad areas in the downstream (Figures 5 and 6), suggesting widely distributed high-pressure basal water.

Pressure melting and frictional heating processes may also generate water beneath the ice in the colder, drier environment of WKS. The thermal regime of a glacier will presumably influence the style of surging as discussed in *Frappé and Clarke* [2007]. The unclear timing of the surge initiation at Svalbard-type glaciers might be attributable to the probably smaller basal water volume available at the time of surge initiation. But we argue here that surface meltwater input does play a role in the dynamics of polythermal glacier surge, even though the water volume is likely smaller than at temperate glaciers.

Sund et al. [2014] describes a surging episode that began in 2003 at the Nathorstbreen glacier system in Svalbard. This system belongs to the Svalbard type due to its estimated ~70 year recurrence interval and 5 year duration of the active phase. However, *Sund et al.* [2014] suggest a different physical surging mechanism, attributing the rapid advance from October 2008 through the following winter to the September rain event, and also suggest a role of englacial water supplied through the newly formed crevasses. Thus, even a Svalbard-type surge may be aided by surface meltwater.

Previous observations of surging glaciers by SAR images have had limited temporal resolutions [*Murray et al.*, 2003; *Quincey et al.*, 2011; *Burgess et al.*, 2012; *Sund et al.*, 2014]. The detection of the winter speedup signals here is due to the high temporal resolution observations in the WKS. Hence, if similarly high-resolution measurements are available elsewhere, similar seasonal modulations would likely be detected.

7. Conclusions

We used LSAT and SAR images from 1972 to 2014 to identify surge-type glaciers in the WKS and to characterize their dynamics. Surge-type glaciers are widely distributed in the WKS, and thus should be included in mass balance studies based on changes in glacier areas, lengths, or ice thicknesses. Surge-type glaciers in the

WKS are characterized by a long (>42 years) recurrence interval and a long (>5 years) duration active phase. These characteristics classify the WKS surges as Svalbard-type surges. Such surges have been presumed to be controlled by the thermal regulation mechanism without surface meltwater input. However, based on the SAR-based surface velocity maps with temporal resolution of down to 11 days, we detected ~200% seasonal velocity modulations with faster speeds in early winter. The winter speedup is similar to the wintertime initiation of the Alaskan-type surge, and thus provides us with evidence for an important role of surface meltwater input and subsequent rerouting through englacial and subglacial drainage system in the generation of such long surges.

Acknowledgments

ERS1/2 and Envisat data are copyrighted by ESA. PALSAR level 1.0 data in this study were provided by the PALSAR Interferometry Consortium to Study our Evolving Land Surface (PIXEL) and the ALOS third PI project under cooperative research contracts with the JAXA. The ownership of PALSAR data belongs to JAXA and the Ministry of Economy, Trade and Industry. TerraSAR-X data are copyrighted by DLR and were provided under TSX proposal LAN1257. ERS1/2 and Envisat data were downloaded from EOLi (https://earth.esa.int/web/guest/eoli), PALSAR data from AUIG2 (https://auig2.jaxa.jp/ips/home), TerraSAR-X data from DLR EOWEB Next Generation (http://eoweb.dlr.de:8080), Landsat images from USGS EarthExplorer (http://earthexplorer.usgs.gov), and SRTM DEM from the CGIAR International Research Centers (http://srtm.csi.cgiar.org). This study is partially supported by JSPS DC-2 fellowship to T.Y. and by KAKENHI (24651001) to M.F. Comments from the Associate Editor, Hester Jiskoot, and three anonymous reviewers were helpful to improve the original manuscript.

References

Abe, T., and M. Furuya (2015), Winter speed-up of quiescent surge-type glaciers in Yukon, Canada, *The Cryosphere*, *9*(3), 1183–1190, doi:10.5194/tc-9-1183-2015.

Bartholomaus, T. C., R. S. Anderson, and S. P. Anderson (2011), Growth and collapse of the distributed subglacial hydrologic system of Kennicott Glacier, Alaska, USA, and its effects on basal motion, *J. Glaciol.*, *57*(206), 985–1002, doi:10.3189/002214311798843269.

Bolch, T., et al. (2012), The state and fate of Himalayan glaciers, *Science*, *336*(6079), 310–314, doi:10.1126/science.1215828.

Bueler, E. (2014), Extending the lumped subglacial-englacial hydrology model of Bartholomaus and others (2011), *J. Glaciol.*, *60*(222), 808–810, doi:10.3189/2014JoG14J075.

Burgess, E. W., R. R. Forster, C. F. Larsen, and M. Braun (2012), Surge dynamics on Bering Glacier, Alaska, in 2008–2011, *The Cryosphere*, *6*(6), 1251–1262, doi:10.5194/tc-6-1251-2012.

Burgess, E. W., R. R. Forster, and C. F. Larsen (2013), Flow velocities of Alaskan glaciers, *Nat. Commun.*, *4*, 2146, doi:10.1038/ncomms3146.

Clarke, G. K. (2005), Subglacial processes, *Annu. Rev. Earth Planet. Sci.*, *33*(1), 247–276, doi:10.1146/annurev.earth.33.092203.122621.

Clarke, G. K. C. (1991), Length, width and slope influences on glacier surging, *J. Glaciol.*, *37*(2), 236–346.

Clarke, G. K. C., J. P. Schmok, C. S. L. Ommanney, and S. G. Collins (1986), Characteristics of surge-type glaciers, *J. Geophys. Res.*, *91*(B7), 7165–7180, doi:10.1029/JB091iB07p07165.

Copland, L., M. J. Sharp, and J. A. Dowdeswell (2003), The distribution and flow characteristics of surge-type glaciers in the Canadian High Arctic, *Ann. Glaciol.*, *36*, 73–81.

Dowdeswell, E. K., J. A. Dowdeswell, and F. Cawkwell (2007), On the glaciers of Bylot Island, Nunavut, Arctic Canada, *Arct. Antarct. Alp. Res.*, *39*, 402–411, doi:10.1657/1523-0430(05-123)[DOWDESWELL]2.0.CO;2.

Eisen, O., W. D. Harrison, C. F. Raymond, K. A. Echelmeyer, G. A. Bender, and J. L. Gorda (2005), Variegated glacier, Alaska, USA: A century of surges, *J. Glaciol.*, *51*(174), 399–406, doi:10.3189/172756505781829250.

Forster, R. R., et al. (2014), Extensive liquid meltwater storage in firn within the Greenland ice sheet, *Nat. Geosci.*, *7*(2), 1–4, doi:10.1038/ngeo2043.

Fountain, A. G., and J. S. Walder (1998), Water flow through temperate glaciers, *Rev. Geophys.*, *36*(3), 299–328, doi:10.1029/97RG03579.

Fowler, A., T. Murray, and F. Ng (2001), Thermally controlled glacier surging, *J. Glaciol.*, *47*(159), 527–538, doi:10.3189/172756501781831792.

Frappé, T. P., and G. K. C. Clarke (2007), Slow surge of Trapridge glacier, Yukon Territory, Canada, *J. Geophys. Res.*, *112*, F03S32, doi:10.1029/2006JF000607.

Gardelle, J., E. Berthier, Y. Arnaud, and A. Kääb (2013), Region-wide glacier mass balances over the Pamir-Karakoram-Himalaya during 1999–2011, *The Cryosphere*, *7*(4), 1263–1286, doi:10.5194/tc-7-1263-2013.

Gardner, A. S., et al. (2013), A reconciled estimate of glacier contributions to sea level rise: 2003 to 2009, *Science*, *340*(6134), 852–857, doi:10.1126/science.1234532.

Grant, K. L., C. R. Stokes, and I. S. Evans (2009), Identification and characteristics of surge-type glaciers on Novaya Zemlya, Russian Arctic, *J. Glaciol.*, *55*, 960–972, doi:10.3189/002214309790794940.

Harper, J. T., J. H. Bradford, N. F. Humphrey, and T. W. Meierbachtol (2010), Vertical extension of the subglacial drainage system into basal crevasses, *Nature*, *467*(7315), 579–582, doi:10.1038/nature09398.

Harrison, W. D., and A. S. Post (2003), How much do we really know about glacier surging?, *Ann. Glaciol.*, *36*(1), 1–6, doi:10.3189/172756403781816185.

Hendriks, J. P. M., and P. P. Helsinki (2007), Semi-automatic glacier delineation from Landsat imagery over Hintereisferner in the Austrian Alps, *Z. Gletscherkd. Glazialgeol.*, *41*, 55–75.

Hewitt, K. (2013), *Glaciers of the Karakoram Himalaya*, 1–452 pp., Advances in Asian Human-Environmental Research, Springer, Netherlands, Dordrecht, doi:10.1007/978-94-007-6311-1.

Iken, A., and M. Truffer (1997), The relationship between subglacial water pressure and velocity of Findelengletscher, Switzerland, during its advance and retreat, *J. Glaciol.*, *43*(1), 328–338.

Jarvis, A., H. Reuter, A. Nelson, and E. Guevara (2008), Hole-filled SRTM for the globe version 4, available from the CGIAR-CSI SRTM 90m Database. [Available at http://srtm.csi.cgiar.org.]

Jiskoot, H., and D. T. Juhlin (2009), Surge of a small East Greenland glacier, 2001–2007, suggests Svalbard-type surge mechanism, *J. Glaciol.*, *55*(191), 567–570, doi:10.3189/002214309788816605.

Jiskoot, H., P. Boyle, and T. Murray (1998), The incidence of glacier surging in Svalbard: Evidence from multivariate statistics, *Comput. Geosci.*, *24*(4), 387–399, doi:10.1016/S0098-3004(98)00033-8.

Jiskoot, H., A. K. Pedersen, and T. Murray (2001), Multi-model photogrammetric analysis of the 1990s surge of Sortebræ, East Greenland, *J. Glaciol.*, *47*(159), 677–687, doi:10.3189/172756501781831846.

Kamb, B. (1987), Glacier surge mechanism based on linked cavity configuration of the basal water conduit system, *J. Geophys. Res.*, *92*(B9), 9083–9100, doi:10.1029/JB092iB09p09083.

Kamb, B., C. F. Raymond, W. D. Harrison, H. Engelhardt, K. A. Echelmeyer, N. Humphrey, M. M. Brugman, and T. Pfeffer (1985), Glacier surge mechanism: 1982–1983 surge of Variegated glacier, Alaska, *Science*, *227*(4686), 469–479, doi:10.1126/science.227.4686.469.

Kobayashi, T., Y. Takada, M. Furuya, and M. Murakami (2009), Locations and types of ruptures involved in the 2008 Sichuan earthquake inferred from SAR image matching, *Geophys. Res. Lett.*, *36*, L07302, doi:10.1029/2008GL036907.

Lingle, C., and D. Fatland (2003), Does englacial water storage drive temperate glacier surges?, *Ann. Glaciol.*, *36*, 14–20, doi:10.3189/172756403781816464.

Luckman, A., D. Quincey, and S. Bevan (2007), The potential of satellite radar interferometry and feature tracking for monitoring flow rates of Himalayan glaciers, *Remote Sens. Environ.*, *111*(2), 172–181, doi:10.1016/j.rse.2007.05.019.

Ma, Q., B. Zheng, K. Jiao, I. Shuji, and H. Fushimi (1989), Glacial geomorphological features in upper reaches of the Yurunkar River on the north slope of the West Kunlun Mountains, *Bull. Glacier Res.*, *7*, 139–144.
Maussion, F., D. Scherer, T. Mölg, E. Collier, J. Curio, and R. Finkelnburg (2014), Precipitation seasonality and variability over the Tibetan plateau as resolved by the high Asia reanalysis, *J. Clim.*, *27*(5), 1910–1927, doi:10.1175/JCLI-D-13-00282.1.
McNabb, R. W., and R. Hock (2014), Alaska tidewater glacier terminus positions, 1948–2012, *J. Geophys. Res. Earth Surf.*, *119*, 153–167, doi:10.1002/2013JF002915.
Meier, M., and A. Post (1969), What are glacier surges?, *Can. J. Earth Sci.*, *6*, 807–817.
Meier, M. F., M. B. Dyurgerov, U. K. Rick, S. O'neel, W. T. Pfeffer, R. S. Anderson, S. P. Anderson, and A. F. Glazovsky (2007), Glaciers dominate eustatic sea-level rise in the 21st century, *Science*, *317*(5841), 1064–1067, doi:10.1126/science.1143906.
Michel, R., J. P. Avouac, and J. Taboury (1999), Measuring near field coseismic displacements from SAR images: Application to the Landers earthquake, *Geophys. Res. Lett.*, *26*(19), 3017–3020, doi:10.1029/1999GL900524.
Moon, T., and I. Joughin (2008), Changes in ice front position on Greenland's outlet glaciers from 1992 to 2007, *J. Geophys. Res.*, *113*, F02022, doi:10.1029/2007JF000927.
Murray, T., G. W. Stuart, P. J. Miller, J. Woodward, A. M. Smith, P. R. Porter, and H. Jiskoot (2000), Glacier surge propagation by thermal evolution at the bed, *J. Geophys. Res.*, *105*(B6), 13,491–13,507, doi:10.1029/2000JB900066.
Murray, T., T. Strozzi, A. Luckman, H. Jiskoot, and P. Christakos (2003), Is there a single surge mechanism? Contrasts in dynamics between glacier surges in Svalbard and other regions, *J. Geophys. Res.*, *108*(B5), 2237, doi:10.1029/2002JB001906.
Neckel, N., J. Kropáček, T. Bolch, and V. Hochschild (2014), Glacier mass changes on the Tibetan Plateau 2003–2009 derived from ICESat laser altimetry measurements, *Environ. Res. Lett.*, *9*(1), 014009, doi:10.1088/1748-9326/9/1/014009.
Pfeffer, W. T., et al. (2014), The Randolph Glacier Inventory: A globally complete inventory of glaciers, *J. Glaciol.*, *60*(221), 537–552, doi:10.3189/2014JoG13J176.
Pritchard, H. (2005), Glacier surge dynamics of Sortebræ, east Greenland, from synthetic aperture radar feature tracking, *J. Geophys. Res.*, *110*, F03005, doi:10.1029/2004JF000233.
Quincey, D. J., M. Braun, N. F. Glasser, M. P. Bishop, K. Hewitt, and A. Luckman (2011), Karakoram glacier surge dynamics, *Geophys. Res. Lett.*, *38*, L18504, doi:10.1029/2011GL049004.
Raymond, C. F. (1987), How do glaciers surge? A review, *J. Geophys. Res.*, *92*(B9), 9121–9134, doi:10.1029/JB092iB09p09121.
Scherler, D., B. Bookhagen, and M. R. Strecker (2011), Hillslope-glacier coupling: The interplay of topography and glacial dynamics in High Asia, *J. Geophys. Res.*, *116*, F02019, doi:10.1029/2010JF001751.
Schoof, C. (2010), Ice-sheet acceleration driven by melt supply variability, *Nature*, *468*(7325), 803–806, doi:10.1038/nature09618.
Shangguan, D., S. Liu, Y. DIng, J. Li, Y. Zhang, L. Ding, X. Wang, C. Xie, and G. Li (2007), Glacier changes in the west Kunlun Shan from 1970 to 2001 derived from Landsat TM/ETM+ and Chinese glacier inventory data, *Ann. Glaciol.*, *46*(1), 204–208, doi:10.3189/172756407782871693.
Strozzi, T., A. Luckman, T. Murray, U. Wegmuller, and C. Werner (2002), Glacier motion estimation using SAR offset-tracking procedures, *IEEE Trans. Geosci. Remote Sens.*, *40*(11), 2384–2391, doi:10.1109/TGRS.2002.805079.
Sund, M., T. R. Lauknes, and T. Eiken (2014), Surge dynamics in the Nathorstbreen glacier system, Svalbard, *The Cryosphere*, *8*(2), 623–638, doi:10.5194/tc-8-623-2014.
Thompson, L. G., E. Mosley-Thompson, M. Davis, P. Lin, J. Dai, J. Bolzan, and T. Yao (1995), A 1000 year climatic ice-core record from the Guliya ice cap, China: Its relationship to global climate variability, *Ann. Glaciol.*, *21*, 175–181.
Truffer, M., W. D. Harrison, and K. A. Echelmeyer (2000), Glacier motion dominated by processes deep in underlying till, *J. Glaciol.*, *46*(153), 213–221, doi:10.3189/172756500781832909.
Wegmüller, U., and C. L. Werner (1997), Gamma SAR processor and interferometry software, in Proceedings of the 3rd ERS Symposium, *Eur. Space Agency Spec. Publ., ESA SP-414*, 1686–1692, European Space Agency, Paris.
Werder, M. A., I. J. Hewitt, C. G. Schoof, and G. E. Flowers (2013), Modeling channelized and distributed subglacial drainage in two dimensions, *J. Geophys. Res. Earth Surf.*, *118*, 2140–2158, doi:10.1002/jgrf.20146.
Yasuda, T., and M. Furuya (2013), Short-term glacier velocity changes at West Kunlun Shan, Northwest Tibet, detected by synthetic aperture radar data, *Remote Sens. Environ.*, *128*, 87–106, doi:10.1016/j.rse.2012.09.021.
Yde, J. C., and O. Y. Paasche (2010), Reconstructing climate change: Not all glaciers suitable, *Eos Trans. AGU*, *91*(21), 189–190, doi:10.1029/2010EO210001.
Zhang, W., R. An, H. Yang, and K. Jiao (1989), Conditions of glacier development and some glacial features in the West Kunlun Mountains, *Bull. Glacier Res.*, *7*, 49–58.
Zhang, Z., and K. Jiao (1987), Modern glaciers on the south slope of West Kunlun Mountains (in Aksayqin Lake and Guozha Co Lake drainage areas), *Bull. Glacier Res.*, *5*, 85–91.
Zheng, B., H. Fushimi, K. Jiao, and S. Li (1989), Characteristics of basal till and the discovery of tephra layers in the West Kunlun Mountains, *Bull. Glacier Res.*, *7*, 177–186.